

## Faulting and Groundwater in Arid Environments: Airborne Electromagnetics in Support of Framework Hydrology in the northern Mojave Desert, southern California

**Paul A Bedrosian**

*United States Geological Survey  
Crustal Geophys. and Geochem. Science Center  
pbedrosian@usgs.gov*

**Jill Densmore-Judy**

*United States Geological Survey  
California Water Science Center  
jdensmo@usgs.gov*

**Peter Martin**

*United States Geological Survey  
California Water Science Center  
pmmartin@usgs.gov*

**Matt Burgess**

*United States Geological Survey  
California Water Science Center  
mburgess@usgs.gov*

**Victoria Langenheim**

*United States Geological Survey  
Geophysical Unit Menlo Park  
zulanger@usgs.gov*

**Robert Jachens**

*United States Geological Survey  
Geophysical Unit Menlo Park  
jachens@usgs.gov*

### SUMMARY

Groundwater basins within the Mojave Desert of the south-western United States are often compartmentalized by faults. As part of an effort to understand and manage groundwater resources in arid environments, the U.S. Geological Survey is investigating a number of basins within the Fort Irwin National Training Center (NTC) using multiple geophysical methods. Gravity, aeromagnetic, ground-based and airborne time-domain electromagnetic (TEM) data were collected over Leach Basin, a geologically complex, internally-drained basin bisected and flanked by Quaternary faults including the Garlock and Death Valley fault zones.

The airborne TEM data show abrupt changes in earth response across faulted boundaries, reflecting the strong resistivity contrast between igneous rocks and basin sediments. The distribution of faults throughout the basin can be directly obtained from the airborne data. A resistivity stratigraphy has been developed by integrating borehole geophysical logs, lab resistivity measurements, and ground-based gravity and TEM soundings. The results are applied to the airborne resistivity models and are used to trace aquifer hydrostratigraphy throughout the basin. Interpreted parameters include the depth to basement, the depth to water, and the thickness of the primary aquifer. Together with hydrologic investigations, these results are being used to estimate groundwater storage within the basin.

**Key words:** hydrogeology; airborne electromagnetics; desert hydrology; Mojave Desert

### INTRODUCTION

Groundwater within the south-western United States is under increasing demand from both irrigation and human consumption. From 2000 to 2005, over 40% of US population growth occurred in arid states, with population in these states increasing by more than 1,000,000. Proposed solar-energy development in the region will add further stress to scarce available water resources. To effectively manage the region's limited groundwater resources there is a need to refine the estimates of available groundwater by defining the size and shape of the groundwater basins and evaluating the water-bearing properties of the basin-fill deposits. Because

numerous faults in the region are barriers to groundwater flow, there is a need to locate buried faults that may compartmentalize the larger groundwater basins into hydraulically isolated subbasins. As part of an effort to understand and manage groundwater resources in arid environments, the USGS is investigating a number of basins within the Fort Irwin National Training Center (NTC) using a multi-method geophysical approach.

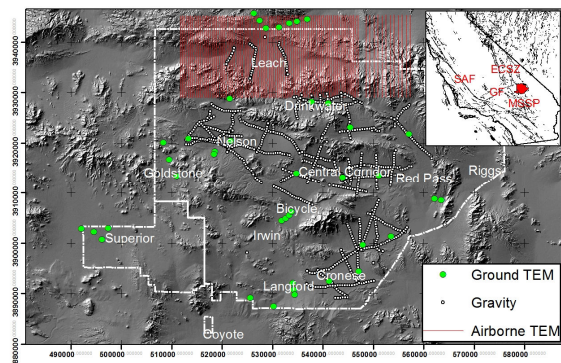


**Figure 1. Geophysical measurements within the Fort Irwin NTC (white outline). GF=Garlock fault; MSSP=Mojave strike-slip province; ECSZ=Eastern California shear zone; SAF=San Andreas fault.**

The NTC is in the northeast part of the Mojave strike slip province (Miller and Yount, 2002) which accommodates late Cenozoic slip along the North American – Pacific plate boundary east of the San Andreas fault. The NTC is cut by numerous faults, including the dextral Death Valley fault zone (DVFZ) and the sinistral Garlock fault (GF); the latter is an important structure accommodating strain between the extensional tectonics of the Basin and Range province and right-lateral motion within the Mojave strike slip province. The study area consists of a series of basins (Figure 1) separated and floored by granitic rocks of Sierran affinity as well as mafic and felsic volcanic and plutonic suites of Tertiary age. These igneous rocks form the base-of-aquifer upon which multiple sedimentary units are overlain (basin-fill deposits). In general, the basin-fill deposits consist of (1) a lower unit (Tog/Tyg) of coarse sands and gravels with secondary clay and calcite, (2) a middle unit (Qoa) of sand, gravel, and clay that is less lithified than the lower unit, and (3) an upper unit (Qya/Qye) of unconsolidated sand and gravel. Clay-rich playa deposits (Qp) are also present at the center of many of the internally-drained basins within the NTC. Excluding Qp, a general decrease in hydraulic

conductivity with increasing depth is recognized within the sedimentary column, however local variations in depositional environment (e.g., provenance and grain size) are reflected in the hydraulic properties of the sediments. Where saturated, the upper unit is the primary aquifer in the NTC basins.

Since 1992 the USGS has been conducting hydrological, geochemical, and geophysical studies of the basins within the NTC. The ultimate goal of these studies is to evaluate the quantity and quality of groundwater in the multiple groundwater basins that underlie the NTC. This paper focuses on the geophysical component, and in particular on an airborne electromagnetic (AEM) study of Leach Basin (Figure 1), a rhomb-shaped fault-bounded basin at the north end of the NTC bisected by the Garlock Fault and terminated to the northeast by the Death Valley Fault Zone. We highlight the use of AEM for mapping hydrostratigraphy in a complex faulted environment. In concert with borehole data, aeromagnetic data, gravity modelling, lab resistivity measurements, and ground TEM data, we are able to estimate basin thickness, internal basin stratigraphy, and the configuration of basin faults and folds. The water table can be mapped locally and recharge and discharge zones can in some cases be identified. This information will be used to estimate the quantity of groundwater storage in the different basins and subbasins and provides primary constraints for future evaluation of the basins using groundwater modelling.

## METHODS

### Electromagnetic measurements

Airborne TEM and magnetic-field data were collected in December, 2010 by Aeroquest Ltd. using the AeroTEM-IV system. 1700 line-kms of data were collected with a nominal line spacing of 400 m. The system consists of a rigid frame transmitter with a moment of 250,000 A·m<sup>2</sup> and a receiver in a central-loop configuration. A triangular bipolar current waveform is employed at a base frequency of 90 Hz with a 50% duty cycle. Usable off-time data span the interval from 100  $\mu$ sec to 3 msec after current turn-off. Navigational data included GPS positioning and a radar altimeter on the helicopter as well as GPS positioning, a laser altimeter, and a 3-component tilt sensor on the transmitter frame.

Ground TEM data were collected at 59 sites throughout the NTC including along a test line at the north edge of Leach Basin (Figure 1). All ground data were collected using a ProTEM system calibrated at the Danish Lyngby test site (Geological Institute, Aarhus University, 2002). The test line was subsequently flown bi-directionally with the AeroTEM system at three flight heights. The airborne test-line measurements were assessed both in the data and model domains. In the data domain we compared measured airborne data to synthetic airborne responses calculated from the inverted ground model. In the model domain we compared co-located inverted ground and airborne models.

A TEM system must be modelled accurately in order to recover realistic subsurface resistivity models (Christiansen et al., 2011). For both ground and airborne TEM systems, we modelled the frequency response of the system, the system geometry, and the current waveform. For the airborne system, the current waveform varies during and between flights (both in timing and amplitude) and is monitored by the contractor;

we modelled a two-pulse waveform that varies dynamically throughout the survey.

AEM data were inverted using the laterally-constrained inversion (LCI) algorithm of Auken et al. (2005). Given the highly-faulted geologic setting, we expected abrupt resistivity contrasts, and hence inverted the data with relatively loose lateral and vertical resistivity constraints imposed on the resulting models. For this same reason, we inverted minimally-processed data (without any smoothing, tie-line levelling, and micro-levelling). Even so, we recognize the limitations of a 1D laterally-constrained approach in this environment and are pursuing 3D inversion of subsets of the data as well as modification of the laterally-constrained approach to incorporate local relaxation of lateral constraints in the vicinity of known or suspected discontinuities.

Due to its use as a year-round live-fire range, ground truth is non-existent within Leach Basin. Well control exists in neighbouring basins, however, and has been used to develop a resistivity stratigraphy. Figure 2 shows a comparison between a TEM ground model, borehole geophysical logs, and laboratory resistivity measurements on borehole spot cores. A clear correlation is observed between the various resistivity estimates. Resistivity breaks are due to both saturation and lithology.

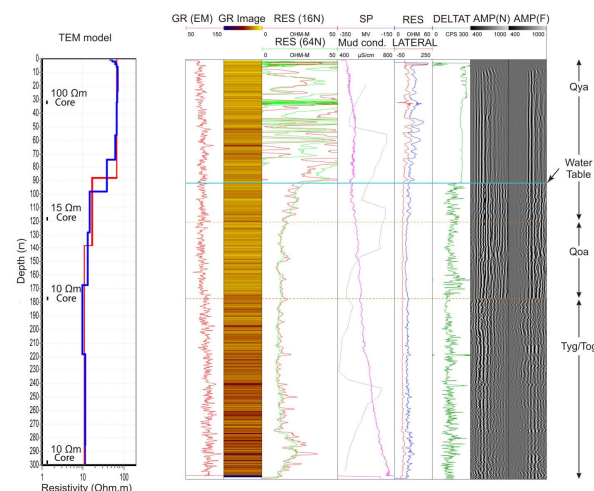


**Figure 2. Ground TEM resistivity model, borehole geophysical logs, and lab resistivity measurements on core from Langford Basin well LL04.**

### Laboratory resistivity measurements

Resistivity measurements were performed on core samples from Langford well LL04 as well as on hand samples of igneous basement rocks to help interpret the TEM data. The resistivity of each sample was measured as collected, after drying, and after saturation. Measurements were made over a frequency range from 100 Hz to 10 KHz.

The spot cores from LL04 include what is interpreted to be Qya, Qoa, Tyg/Tog. The sample of Qya is moderately resistive (100  $\Omega$ -m) when dry, but exhibits a distinctly lower resistivity (40  $\Omega$ -m) when saturated. In contrast, samples of Qoa, Tyg and Tog are all conductive (10-20  $\Omega$ -m), irrespective of the degree of saturation. These measurements are of great importance in interpreting the airborne resistivity models. Where the water table is within the younger Quaternary

sediments (Qya) a distinct break in resistivity is expected. If, however, the water table falls within the older basin-fill deposits (Qoa, Tyg, Tog) this boundary is all but invisible in the resistivity models.

Laboratory resistivity measurements on the basement rocks are all resistive ( $> 1,000 \Omega\cdot\text{m}$ ), however Tertiary volcanic rocks on average have resistivities an order of magnitude higher ( $10,000 \Omega\cdot\text{m}$ ) than Mesozoic intrusive rocks ( $1,000 \Omega\cdot\text{m}$ ). This difference is observed indirectly in the AEM data, where measurements over mapped intrusive rocks show a measurable, albeit small, response at early times. In contrast, measurements over mafic volcanic and plutonic rocks entrained within the Garlock Fault have no measurable response, even at the earliest time gates. Felsic volcanic rocks in the southeast corner of the survey area (Figure 3c) have resistivities intermediate between the Mesozoic intrusive rocks and the mafic volcano-plutonic rocks.

### Gravity data

Gravity data were collected along three profiles through Leach Basin (Figure 1) to supplement sparse, previously available measurements. The gravity data were reduced to isostatic anomalies using a reduction density of  $2,670 \text{ kg/m}^3$  and include earth-tide, instrument drift, free-air, Bouguer, latitude, curvature, and terrain corrections (Telford and others, 1976). An isostatic correction using a sea-level crustal thickness of 25 km and a mantle-crust density contrast of  $400 \text{ kg/m}^3$  was applied to the data to remove the long-wavelength gravitational effect of isostatic compensation of the crust due to topographic loading. The thickness of the valley-fill deposits (or depth to the basement complex) throughout the study area was estimated using the method of Jachens and Moring (1990), modified slightly to permit inclusion of constraints at points where the thickness of the valley-fill deposits is known from direct borehole observations. The density-depth relationship used to calculate thickness is a four-layer model based on well data throughout the Basin and Range (Jachens and Moring, 1990).

## RESULTS

Figure 3 shows representative north-south resistivity cross-sections through (a) the center of Leach Basin and (b) near the intersection of the GF and the DVFZ. These cross-sections reflect the geologic and hydrologic structure within Leach Basin and the faults that bound and bisect it. The basin center profile images a thin surface conductor associated with clay-rich playa deposits of pluvial Leach Lake (1). The Garlock fault (2) is imaged as a sharp discontinuity in the resistivity model. The lithologic contrast between younger Quaternary sediments and older basin-fill deposits is a prominent boundary (3) imaged discontinuously throughout the basin. Tight folding of this boundary is identified on the north end of the basin (4), in addition to faulting along over-steepened fold limbs. Both the topography of this boundary and the imaged resistivity contrast ( $60\text{-}100 \Omega\cdot\text{m}$  over  $10 \Omega\cdot\text{m}$ ) indicate that this boundary is a lithologic rather than hydrologic boundary between the upper and middle units of the basin fill deposits. The water table (5) is a more subtle resistivity contrast ( $60\text{-}100 \Omega\cdot\text{m}$  over  $40 \Omega\cdot\text{m}$ ), is consistent with the lab measurements, and is only identified where it intersects Qya. An uplift of basement rocks within the southern basin (6) is moderately resistive; magnetic data (Figure 4d) suggests mafic

volcanic or plutonic rocks. A fault-bounded basement block (7) is also imaged on the north end of the basin.

The eastern profile (Figure 3b) spans 1,200 m of surface elevation and images faulting and folding associated with the DVFZ. Tertiary mafic rocks of the Avawatz Mountains (2) are distinctly more resistive than Mesozoic felsic rocks of the Granite Mountains (3). This distinction between mafic and felsic rocks is observed throughout the survey area, and in combination with their different magnetic signatures (Figure 4d) permits discrimination of these rocks. Folded sediments are imaged within a hanging basin (4), and resistive sediments on the south end of this basin (5), interpreted to be alluvium derived from the weathered granites upslope, are offset by a series of faults.

The features observed in cross-section can be traced throughout the basin in Figure 4, which shows (a) generalized geology, (b) basin thickness, (c) resistivity at 50 m depth, and (d) magnetic field anomaly. The Granite Mountains (1) are characterized by a rough texture in both resistivity and magnetic-field maps. The basement high (2) correlates with thin basin fill, higher resistivity, and a high magnetic-field anomaly, suggestive of mafic basement rocks. Linear features along the GF (3) and DVFZ (4) reflect slivers of igneous and siliciclastic basement rock entrained within these fault zones. A localized depocenter (5) is recognized at the west end of Leach Basin, with higher resistivity reflecting a thicker package of unsaturated Qya. A thick sedimentary section is suggested by gravity data along the DVFZ (6), which reflects thickened Tertiary sediments that have been folded and faulted. Mafic volcanic rocks, with a characteristic high magnetic-field signature, appear to be faulted in a left lateral sense across the Owl Lake Fault (7). Volcanic rocks in the southeast corner of the basin (8) exhibit a similar magnetic field signature. A structural arch (9) can be seen sub-parallel to and north of the Garlock Fault, where conductive Tertiary sediments are strongly folded, gravity-derived thickness estimates are low, and a magnetic field high suggests shallow basement. Finally, the hanging basin between the Granite and Avawatz Mountains (10) appears as a local depocenter and is supported by a subdued magnetic-field and resistivity signature relative to the surrounding ranges.

## CONCLUSION

AEM models, together with other geophysical data, provide a wealth of information on basin hydrogeology, subsurface geology, and faulting within a complex environment. In the future, resistivity cross-sections will be used to initialize potential-field models. These data sets are complimentary in that magnetic-field data are able to distinguish between felsic and mafic compositions. Similarly, gravity provides important constraints on the depth to basement that is typically well beyond the AEM depth-of-investigation.

Future work involves incorporating geologic and geophysical information within a 3D EarthVision model, together with hydrologic information (e.g. hydraulic conductivity) from nearby accessible basins. This model will aid in understanding the compartmentalization of groundwater within Leach Basin, as well as providing direct input for the estimation of groundwater storage and the development of basin groundwater models.

## REFERENCES

Auken, E., A.V. Christiansen, B.H. Jacobsen, N. Foged, and K.I. Sørensen, 2005, Piecewise 1D laterally constrained inversion of resistivity data: *Geophys. Prospect.*, 53, 497–506.

Christiansen, A.V., E. Auken, and A. Viezzoli, 2011, Quantification of modeling errors in airborne TEM caused by inaccurate system description: *Geophysics*, 76, f43-f52.

Christiansen, A.V. and E. Auken, 2010, A global measure for depth of investigation in EM and DC modeling, Australian Soc. Explor. Geophys. Conference and Exhibition, Sydney.

Geological Institute, 2002, Vejledning i kalibrering af TEM måleudstyr (in Danish): Aarhus University, 12p.

Jachens, R.C. and B.C. Moring, 1990, Maps of the thickness of Cenozoic deposits and the isostatic residual gravity over basement for Nevada: U.S. Geological Survey Open-File Report 90-404, 15 p., 2 plates.

Miller, D.M. and J.C. Yount, 2002, Late Cenozoic tectonic evolution of the north-central Mojave Desert inferred from fault history and physiographic evolution of the Fort Irwin area, California, in Glazner, A.F., Walker, J.D., and Bartley, J.M., eds., *Geologic Evolution of the Mojave Desert and Southwestern Basin and Range*: Boulder, Colorado, Geol. Soc. Amer. Memoir 195, p. 173-197.

Saucedo, G.J., D.R. Bedford, G.L. Raines, R.J. Miller, and C.M. Wentworth, 2000, GIS data for the geologic map of California: California Division of Mines and Geology CD 2000-007.

Telford, W.M., L.O. Geldart, R.E. Sheriff, and D.A. Keyes, 1976, *Applied Geophysics*: New York, Cambridge University Press, 960 p.

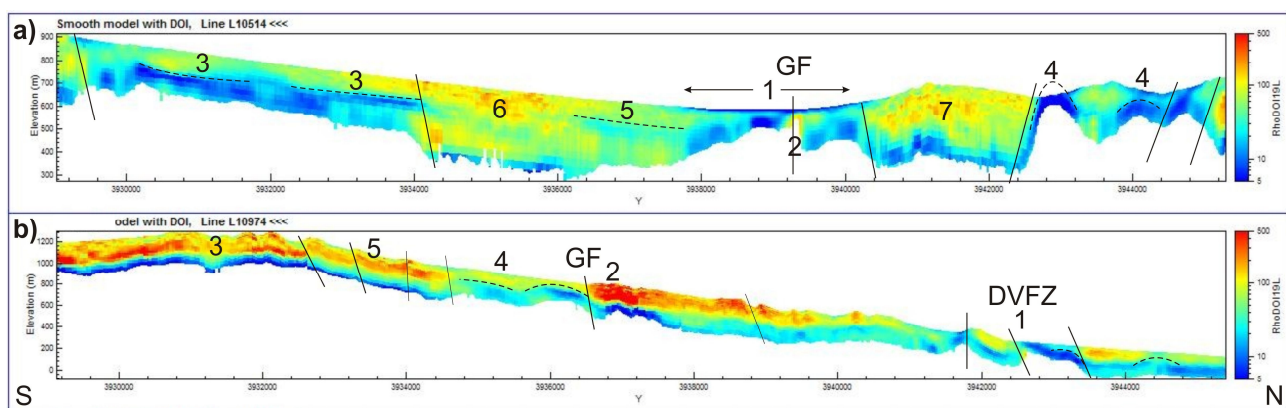


Figure 3. Resistivity cross-sections through a) the center of Leach Basin and b) near the intersection of the Garlock Fault (GF) and Death Valley Fault Zones (DVFZ). Profile locations are identified in Figure 4a. Numbered features are discussed in the text. Cross-sections are terminated at depth based upon a depth-of-investigation metric (Christiansen and Auken, 2010).

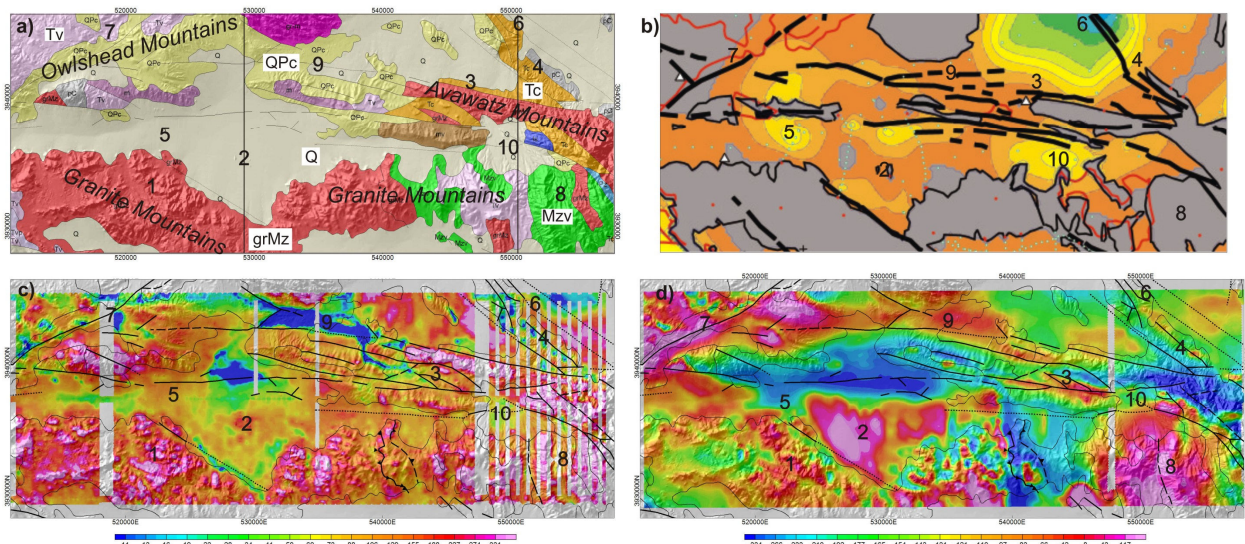


Figure 4. Geophysical images of Leach Basin. a) generalized geology from Saucedo et al. (2000) b) gravity-derived basin thickness as 100 m contours, grey = no or minimal sediments; dark orange = less than 100 m sediments, blue = 800-900 m sediments, c) electrical resistivity at 50 m depth, d) IGRF removed magnetic-field anomaly. Q = Quaternary alluvium; QPc = Plio-Pleistocene nonmarine; Tc = Tertiary nonmarine; Tv = Tertiary volcanic rocks; grMz = Mesozoic granitic rocks; Mzv = Mesozoic volcanic and metavolcanic rocks. Numbered features are discussed in the text.